



## Hydrothermal evolution of PF-co-doped TiO<sub>2</sub> nanoparticles and their antibacterial activity against carbapenem-resistant *Klebsiella pneumoniae*



László Kőrösí<sup>a,\*</sup>, Balázs Bognár<sup>b</sup>, Marianna Horváth<sup>c</sup>, György Schneider<sup>c</sup>, János Kovács<sup>d</sup>, Alice Scarpellini<sup>e</sup>, Andrea Castelli<sup>f</sup>, Massimo Colombo<sup>f</sup>, Mirko Prato<sup>g,\*</sup>

<sup>a</sup> Research Institute for Viticulture and Oenology, University of Pécs, Pázmány Péter u. 4, H-7634 Pécs, Hungary

<sup>b</sup> Institute of Organic and Medicinal Chemistry, University of Pécs, Szigeti st. 12, H-7624 Pécs, Hungary

<sup>c</sup> Department of Medical Microbiology and Immunology, Medical School, University of Pécs, Szigeti st. 12, H-7624 Pécs, Hungary

<sup>d</sup> Environmental Analytical and Geoanalytical Research Group, Szentágóthai Research Centre, University of Pécs, Ifjúság u. 20, H-7624 Pécs, Hungary

<sup>e</sup> Electron Microscopy Facility, Istituto Italiano di Tecnologia, via Morego 30, 16163 Genova, Italy

<sup>f</sup> Department of Nanochemistry, Istituto Italiano di Tecnologia, via Morego 30, 16163 Genova, Italy

<sup>g</sup> Materials Characterization Facility, Istituto Italiano di Tecnologia, via Morego 30, 16163 Genova, Italy

### ARTICLE INFO

#### Keywords:

TiO<sub>2</sub>  
Nonmetal co-doping  
Photocatalysis  
Antibacterial activity  
EPR

### ABSTRACT

Carbapenem-resistant *Klebsiella pneumoniae* (CP-Kp) is one of the most important opportunistic pathogens strongly associated with nosocomial infections. The capsule of CP-Kp not only contributes to its pathogenic potential but also ensures survival for bacteria in different environments and surfaces. Development of novel reactive nanomaterials can help to inhibit the survival of such microorganism and thereby their spreading in the hospital environment. In this work, the photocatalytic and antibacterial activities of PF-co-doped anatase TiO<sub>2</sub> nanoparticles (NPs) were studied in details and related to the evolution of their structure and surface composition upon hydrothermal treatment at 250 °C for periods up to 12 h. Structural and morphological evolution were followed by X-ray diffraction, transmission electron microscopy while the surface composition was studied by X-ray photoelectron spectroscopy. Electron paramagnetic resonance measurements were carried out to reveal the formation of reactive oxygen species (ROS). Both OH· and O<sub>2</sub>·<sup>-</sup> radicals as well as <sup>1</sup>O<sub>2</sub> were confirmed and quantitatively compared in different photoirradiated PF-TiO<sub>2</sub> NPs dispersions. It was found that hydrothermal treatment increased the photocatalytic and antibacterial activity while PF-co-doping promoted the formation of OH· radicals. By the application of PF-co-doping, the elevated level of OH· led to rapid inactivation of CP-Kp.

### 1. Introduction

Carbapenem-resistant *Klebsiella pneumoniae* (CR-Kp) is an emerging multi-drug resistant pathogen. It is mostly associated with urinary, respiratory and bloodstream infections in patients with underlying medical conditions. CR-Kps are able to produce carbapenemases, i.e. enzymes that hydrolyze carbapenems, often the last antibiotic resort for resistant Gram-negative infections [1]. Infections with CR-Kps represent a significant public health challenge since they more often lead to therapeutic failures and result in high hospitalization costs [2]. Their spread in the hospital environments is mostly supported by their capsule, a cell surface component, that not only contributes to the pathogenic potential and antibiotic resistance but also assures survival on different surfaces [3]. Thus, development of bactericidal surface treatments and of novel materials with antibacterial features is very timely and justified.

For this purpose, reactive nanoparticles seem to be potential candidates. Indeed, reactive oxygen species (ROS) such as superoxide radical anion (O<sub>2</sub>·<sup>-</sup>) and hydroxyl radicals (OH·) can be generated on photocatalytically active TiO<sub>2</sub> nanoparticles (NPs) irradiated by photons with appropriate energy, in most cases with UV light [4,5]. The produced ROS are very effective tools both in the degradation of harmful compounds and in the inactivation of pathogens [6]. Enhancing the efficiency of ROS generation on semiconductor metal oxide NPs (i.e. improving the photocatalytic activity) is one of the major goals in heterogeneous photocatalysis. Among metal oxides, TiO<sub>2</sub> (a wide-band-gap semiconductor) shows high photocatalytic activity. To decrease its band gap energy, thus allowing to exploit its photocatalytic activity also with visible light irradiation, doping with various elements is frequently applied. Non-metal doping is a very promising strategy for the preparation of TiO<sub>2</sub> with enhanced photocatalytic performance. Doping with p-block elements such as B, C, N, F and P is intensively

\* Corresponding authors.

E-mail addresses: korosi.laszlo@pte.hu (L. Kőrösí), mirko.prato@iit.it (M. Prato).

studied in semiconductor photocatalysis [7–11]. Although the band gap narrowing or visible light absorption of  $\text{TiO}_2$  can be readily achieved by doping, the addition of dopants frequently decreases the photocatalytic activity because the dopants can act as recombination centers for the charge carriers, that are no more available for generation of ROS species [12,13]. Moreover, the introduction of electronic states above the valence band decreases the oxidation power under visible light irradiation [14]. Based on the numerous theoretical and experimental studies, co-doping may offer new alternatives and solutions [15–19]. For example, both F-N and P-N co-doped titania exhibited higher photocatalytic activity than that of single doped  $\text{TiO}_2$  [20,21]. It was found that N atoms enhanced the visible light absorption while the F increased the adsorption of organic substances and improved the charge separation efficiency [22]. PN-co-doping resulted in a significant improvement in the separation of photo-excited electrons and holes and enables the nitrogen-doping  $\text{TiO}_2$  to catalyze the overall splitting of water into molecular hydrogen and oxygen [23]. The synergistic effect of different dopants was also evident when the photocatalysts were tested in the degradation of various pollutants, such as organic dyes [24]. Previously, we demonstrated that co-doping of  $\text{TiO}_2$  with P and F significantly increased the rate of photodegradation of methyl orange if the dopant concentration was kept in the appropriate range [25].

In this work, we further investigate the influence of the duration of the hydrothermal treatment on the crystallinity, morphology, chemical composition and antibacterial activity of PF-TiO<sub>2</sub> NPs. The structural and morphological evolution were followed by X-ray diffraction (XRD) and transmission electron microscopy (TEM), respectively, meanwhile the near surface region was monitored by X-ray photoelectron spectroscopy (XPS). We studied in detail the formation of ROS in the photocatalytic systems by means of electron paramagnetic resonance (EPR) measurements. Photocatalytic activity was studied on the degradation of methyl orange in PF-TiO<sub>2</sub> NPs dispersions. The antibacterial activity of PF-TiO<sub>2</sub> NPs was tested against the CR-Kp 53/3 strain.

## 2. Experimental

### 2.1. Materials

2-Propanol (HiPerSolv CHROMANORM for HPLC, VWR)  $\text{TiCl}_4$  ( $\geq 98\%$ , Fluka), NaOH (99.9%, Molar Chemicals Ltd., Hungary), HPF<sub>6</sub> (55 wt%, Sigma-Aldrich),  $\text{NaHCO}_3$  (ACS reagent, 99.7%, Sigma-Aldrich), HCl (ARISTAR®, 37%, VWR), methyl orange (ACS reagent, Alfa Aesar), Dimethyl sulfoxide, DMSO ( $\geq 99.9\%$ , Sigma-Aldrich), 4-oxo-2,2,6,6-tetramethylpiperidine, TMPO, (99.4%, Molar Chemicals Ltd., Hungary) were used as received. 5,5-dimethyl-1-pyrroline *N*-oxide, DMPO, was synthesized as previously described [26], and it was freshly distilled prior to use.

VIM 53/3 strain was a carbapenem-resistant stool isolate [27]. Luria Broth (LB) medium was prepared by using yeast extract (Oxoid, USA), bacto peptone (Oxoid, USA), NaCl (analytical reagent, Reanal, Hungary) and deionized water.

For all experiments, high purity deionized water was obtained by a LaboStar™ 7 TWF-UV (Germany) system.

### 2.2. Synthesis

50 mL of 2-propanol was added carefully to 23 g of  $\text{TiCl}_4$ . Caution! Because of the violent, exothermic reaction this procedure should be performed in a fume hood. After the subsequent sonication for 5 min, a transparent, yellow solution was formed. 100 mL of high purity deionized water was added to the mixture resulting in a clear, colorless solution. For the hydrolysis of Ti precursors, 250 mL of 1.5 M NaOH solution was added dropwise to the above system under vigorous stirring. The obtained white precipitate was thoroughly washed and then dispersed in 400 mL of deionized water. Thereafter, 7.3 mL of 0.38 mol/L HPF<sub>6</sub> solution was added to the dispersion during stirring. The HPF<sub>6</sub>

treatment was carried out at 25 °C for 30 min. 50 mL aliquots of the dispersion were treated hydrothermally at 250 °C for 1, 3, 6 or 12 h. The dispersions were centrifuged and then washed with deionized water and 2-propanol. Finally, the obtained sediments were dried at 50 °C in air.

### 2.3. $\text{NaHCO}_3$ treatment on PF-TiO<sub>2</sub> NPs

0.5 g of the PF-TiO<sub>2</sub> sample treated hydrothermally for 12 h (PF-TiO<sub>2</sub>/12 h in the following) was dispersed in 50 ml of 1 M  $\text{NaHCO}_3$  solution, and the resulting dispersion was stirred at 70 °C for 2 h. The treated NPs were centrifuged at room temperature and washed with deionized water for several times. To remove  $\text{NaHCO}_3$  residue, the sediment was redispersed in 50 ml of 0.1 M HCl. The washing procedure was continued with deionized water until the supernatant was free of chloride ions (using  $\text{AgNO}_3$  test). Finally, NPs were washed with 2-propanol, and dried at 50 °C in air.

### 2.4. Characterization

XRD patterns were collected using a Rigaku MiniFlex 600 X-ray diffractometer equipped with a Cu  $\text{K}\alpha$  anode operated at 40 kV and 15 mA. Transmission electron microscopy (TEM) images were obtained with a JEOL JEM-1011 electron microscope equipped with a W thermionic electron source at an accelerating voltage of 100 kV. TEM images were collected using a Gatan SC-1000 Orius CCD Camera and recorded (and also post-processed) using the Digital Micrograph software by Gatan. The data have been then statistically analyzed using OriginPro 9.1. XPS measurements were performed on a Kratos Axis Ultra<sup>DLD</sup> spectrometer, using a monochromatic Al  $\text{K}\alpha$  source operated at 15 kV and 20 mA. High-resolution narrow scans were acquired on O 1s and Ti 2p core levels, as well as on the F 1s and P 2p ones, at constant pass energy of 10 eV in steps of 0.1 eV. The photoelectrons were detected at a take-off angle of  $\phi = 0^\circ$  with respect to the surface normal. The data were processed with CasaXPS software, version 2.3.16. The binding energy (BE) scale was internally referenced to the C 1s peak (BE for C—C = 284.8 eV). Diffuse reflectance spectra were collected with a Varian Cary 5000 UV-vis-NIR spectrophotometer equipped with an External Diffuse reflectance – 2500 accessory and operating in reflectance geometry. Specific surface area and porosity measurements were carried out by nitrogen physisorption at 77 K in a Quantachrome equipment, model autosor iQ. Prior to measurements, samples were degassed for 3 h at 150 °C under vacuum to eliminate weakly adsorbed species. The specific surface areas were calculated using the multi-point BET (Brunauer–Emmett–Teller) model, considering 11 equally spaced points in the P/P<sub>0</sub> range from 0.05 to 0.30. EPR spectra were recorded on Miniscope MS 200 spectrometer with modulation amplitude of 0.2 mT and microwave power of 10.0 mW, the value of receiver gain was 500. Measurements were carried out in water (for  $\text{OH}^\cdot$  and  ${}^1\text{O}_2$ ) or DMSO (for  $\text{O}_2^\cdot$ ) containing 100 mg/L of PF-TiO<sub>2</sub> NPs. Concentrations of spin traps were 100 mM of DMPO or 10 mM of TMPO. EPR spectra were monitored upon photoirradiation using a 15-W UV-A light source for 20, 40, 60, 80, 100, 180, 300, 600, and 1200 s in the case of  $\text{OH}^\cdot$ , and  $\text{O}_2^\cdot$  or 2, 5, 10, 20, 30, 45 min in the case of  ${}^1\text{O}_2$ .

### 2.5. Photocatalytic tests

The photocatalytic activities of PF-TiO<sub>2</sub> NPs were tested by the photodegradation of methyl orange (MO). For the photocatalytic tests, 50 ml of 0.05 w/v% aqueous PF-TiO<sub>2</sub> NPs dispersions containing 10 mg/l MO were used. Prior to the light exposure, the suspensions were stirred in the dark for 60 min in order to allow the adsorption to reach equilibrium. The dispersions were covered with glass lids of Petri dishes, and then irradiated at room temperature for different time by using a 15-W UV-A light source (F15W T8 BL368, Sylvania). The working distance was 5 cm. Before analysis, the dispersions were

centrifuged at  $20,660 \times g$  for 10 min. The concentration of MO was determined by UV-vis spectroscopy (Shimadzu UV-1800).

## 2.6. Antibacterial tests

The CR-Kp 53/3 strain was used to demonstrate the antibacterial effects of the different PF-TiO<sub>2</sub> NPs. Tests were performed as previously described with slight modifications [27]. Briefly, 5 mL of the overnight cultures in Luria Broth medium (LB) were collected with centrifugation at  $10,000 \times g$ , for 2 min, washed twice with 0.9 w/v% NaCl solution and optical densities were set to OD<sub>600</sub> = 1 ( $1 \times 10^8$  CFU/mL). Tests were carried out in 100 mL beakers containing 9.9 mL PF-TiO<sub>2</sub> NPs dispersions and 100 μL bacterium suspensions. The final concentration of PF-TiO<sub>2</sub> NPs and bacteria were 0.05 w/v% and  $\sim 10^6$  CFU/mL, respectively. After mixing the PF-TiO<sub>2</sub> and the bacterial suspensions, the mixtures in beakers were stirred on a parallel magnetic stirrer platform installed in a closed dark box especially constructed for our purposes. After 30 min of dark preincubation, the photocatalytic reactions were started by switching on a 15-W UV-A lamp (F15W/T8/BL368 fluorescent lamp, Sylvania). For bacterial enumeration, 10 μL of sample aliquots were taken at 0, 15, 30, 45 and 60 min. The numbers of viable cells were determined by oozing 10 μL of suitably diluted aliquots onto LB agar plates and then counting the colonies after 24 h of incubation at 37 °C.

## 3. Result and discussion

### 3.1. Crystal structure

XRD patterns of PF-TiO<sub>2</sub> samples prepared at different times of hydrothermal treatment are presented in Fig. 1. All diffraction peaks are in good agreement with JCPDS card No. 78-2486, indicating that our NPs crystallized in the anatase phase. Increasing the hydrothermal treatment duration, the intensity of the XRD peaks increased while their full-width at half maximums (FWHM) decreased (Table 1). This shrinking of FWHM is indicative of a hydrothermal-treatment-induced crystal growth. Indeed, the average crystallite size calculated via Scherrer equation was 5.7, 10.4, 12.0, 17.7 and 23.9 nm after hydrothermal treatment at 250 °C for 0, 1, 3, 6 and 12 h, respectively. Anatase contents of the samples were estimated by the areas of  $d_{101}$  peak, using an external anatase TiO<sub>2</sub> standard. Interestingly, without the application of hydrothermal treatment sample (henceforth abbreviated as PF-TiO<sub>2</sub>/0 h) showed relatively high crystallinity demonstrating 76 wt% anatase and 24 wt% amorphous phase. Crystallinity increased sharply

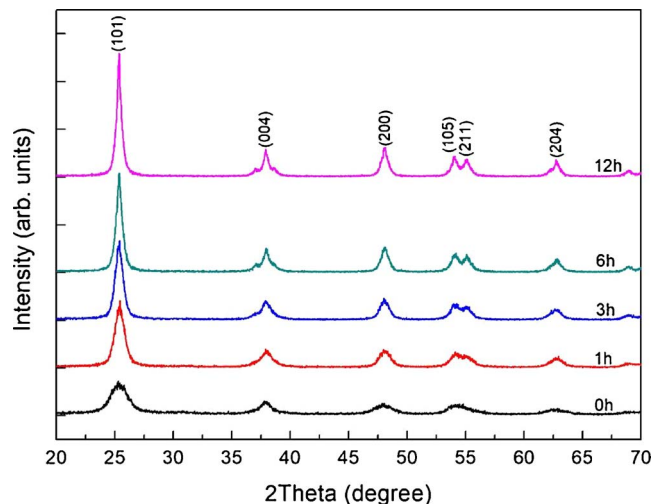


Fig. 1. XRD patterns of PF-TiO<sub>2</sub> samples treated hydrothermally at 250 °C for different time periods.

Table 1

Crystallite size and crystallinity of PF-TiO<sub>2</sub> samples treated hydrothermally for different time.

Treatment time (h)	FWHM	D <sup>a</sup> (nm)	Area of $d_{101}$ peak (a.u.)	Anatase wt%	Amorphous wt%
0	1.52	5.7	583	76	24
1	0.88	10.4	715	93	7
3	0.78	12.0	730	95	5
6	0.56	17.7	743	97	3
12	0.44	23.9	768	100	0

<sup>a</sup> Average crystallite diameter (D) determined using the Scherrer equation from the full width at half maximum of the  $d_{101}$  peak.

with the treatment time and the anatase content reached 95 wt% after 3 h. As we expected, the highest crystallinity was observed after hydrothermal treatment of 12 h (Table 1).

### 3.2. Dopants distribution at the near-surface region

The chemical composition of the near-surface region of PF-TiO<sub>2</sub> samples prepared with different time of hydrothermal treatment has been studied by means of XPS. The results obtained on the energy regions typical for Ti 2p, O 1s, F 1s and P 2p are shown in Fig. 2, after normalization to the Ti 2p<sub>3/2</sub> peak area.

For all the samples, the main Ti and O peaks (centered respectively at  $458.7 \pm 0.2$  eV and at  $529.9 \pm 0.2$  eV) are characteristic of Ti<sup>4+</sup> oxide. Moreover, in all the cases O 1s peak is clearly asymmetric, due to the presence of low intensity components at the high-binding-energy side of the main O peak. These minor oxygen components are centered at approx. 530.7 eV, 531.6 eV and 532.8 eV, and could be assigned respectively, to O atoms in the P=O/Ti—O—P environments, to —OH groups at the sample surface, and to molecular water adsorbed on the surface of the NPs [28,29]. The positions of each O sub-component,

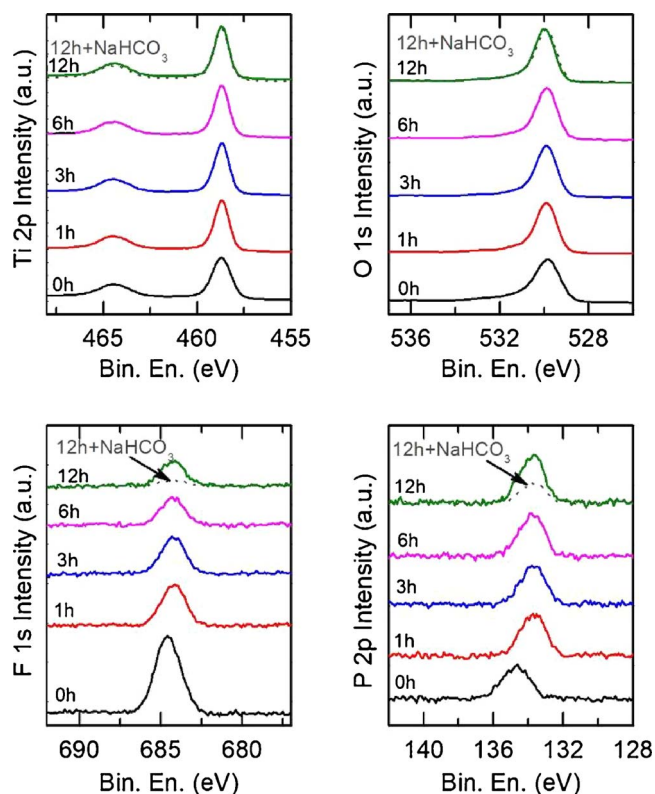


Fig. 2. High-resolution XP spectra of PF-TiO<sub>2</sub> NPs with different hydrothermal treatment time.

**Table 2**

Chemical environments of O sub-components with their relative concentrations.

Sample ID	Lattice O	P=O/Ti–O–P	–OH	Adsorbed water
0 h	529.8 eV (77.7%)	530.9 eV (12.1%)	531.8 eV (6.4%)	532.9 eV (3.8%)
1 h	529.9 eV (82.3%)	530.9 eV (9.7%)	531.7 eV (5.3%)	532.9 eV (2.7%)
3 h	529.9 eV (81.3%)	530.7 eV (10.0%)	531.5 eV (6.1%)	532.8 eV (2.6%)
6 h	529.9 eV (80.8%)	530.6 eV (9.8%)	531.5 eV (6.9%)	532.7 eV (2.5%)
12 h	529.8 eV (80.1%)	530.5 eV (11.5%)	531.4 eV (6.6%)	532.8 eV (1.8%)
12 h + NaHCO <sub>3</sub>	529.8 eV (80.2%)	530.7 eV (10.3%)	531.6 eV (6.6%)	532.8 eV (2.9%)

**Table 3**The effect of the duration of hydrothermal treatment on the surface composition of PF-TiO<sub>2</sub> NPs.

Sample ID	Ti (at%)	O (at%)	F (at%)	P (at%)	F/P	P/Ti
0 h	27.6	65.2	6.2	1	6.2	0.036
1 h	29.5	65.9	3.3	1.2	2.8	0.041
3 h	29.7	66.2	3.1	1	3.1	0.034
6 h	29.5	67.3	2.1	1.1	1.9	0.037
12 h	29.3	67.3	2.1	1.3	1.6	0.044
12 h + NaHCO <sub>3</sub>	30.4	68.3	0.6	0.6	1	0.020

together with their relative concentration, are summarized in **Table 2**. The position of F 1s peak is found to slightly shift from  $684.6 \pm 0.2$  eV before hydrothermal process to  $684.3 \pm 0.2$  eV after the treatment. We assign this peak to F<sup>−</sup> that are adsorbed on the surface of TiO<sub>2</sub> NPs ( $\equiv$ Ti–F) [30]. On the other hand, P 2p peaks show a higher shift after hydrothermal treatment. The main component P 2p<sub>3/2</sub> shifted from  $134.5 \pm 0.2$  eV to  $133.6 \pm 0.2$  eV suggesting that the P<sup>5+</sup> replaced a part of Ti<sup>4+</sup> in the crystal lattice of TiO<sub>2</sub> [31].

The results of the quantitative analysis are summarized in **Table 3**, where the relative atomic concentration of Ti, O, F and P are reported. If no hydrothermal treatment is applied to the as-prepared PF-TiO<sub>2</sub> NPs (sample 0 h), the F:P ratio resembles that of the PF<sub>6</sub><sup>−</sup> moiety, used for PF-co-doping. As the hydrothermal treatment time was increased, the F:P ratio decreased, reaching a value of 1.6 after 12 h of treatment. This observation suggests that, under our experimental conditions, the PF<sub>6</sub><sup>−</sup> moiety decomposed into separate P and F groups, and also suggests that P has higher affinity and higher thermal stability on the TiO<sub>2</sub> surface than that of F since the P:Ti ratio is almost constant for all the studied samples at approx. 0.04. The XPS results, therefore, indicate that PF<sub>6</sub><sup>−</sup> species adsorbed on TiO<sub>2</sub> NPs at room temperature, and then only F partially desorbed at 250 °C. Longer treatment time favours the F-desorption.

In order to reveal the importance of P and F moieties at the surface of PF-TiO<sub>2</sub> NPs, we treated the sample obtained after 12 h of hydrothermal synthesis with NaHCO<sub>3</sub> and then performed XPS investigation. The results, reported in **Table 3**, show that the atomic concentration of both P and F decreased to 0.6 at% after the NaHCO<sub>3</sub> treatment. After this treatment the original crystal phase did not change and there was no significant difference in FWHM of anatase  $d_{101}$  peaks before and after the treatment, demonstrating the similar average crystallite size for both samples (Fig. S1 in the Supplementary material). Thus, any differences in the photocatalytic or antibacterial activity of the treated and untreated PF-TiO<sub>2</sub>/12 h NPs should be related to the near-surface composition, i.e. the presence or the absence of PF-dopants.

### 3.3. Optical properties

As shown in Fig. S2, the color of the investigated powder samples moves from white to light blue, as a function of the hydrothermal treatment duration. In agreement with previous reports in literature [32,33], this observation suggests that the hydrothermal treatment together with doping is favoring the formation of oxygen vacancies and consequently of self-doping by Ti<sup>3+</sup> species, known to exhibit visible

light response. However, considering the outcome of our XPS analysis, showing only signals ascribable to Ti<sup>4+</sup> at the surface of the investigated samples, we could speculate that these reduced Ti species are localized in the core of our particles. To get more insights in the presence of these species, we collected diffuse reflectance spectra on all the considered samples. The results are reported in Fig. S3; the absorption onset changes only slightly (few meV) as a function of the hydrothermal treatment duration, similar to what observed by Xu et al. [32] for low doping regime.

### 3.4. Size and morphology

The particle size and morphology of the PF-TiO<sub>2</sub> samples were analysed by TEM in bright field mode. TEM image of sample PF-TiO<sub>2</sub>/0 h shows irregular, tiny particles in amorphous matrix, whereas hydrothermal treated PF-TiO<sub>2</sub> NPs are polymorphic exhibiting spherical, polyhedral and elongated morphology (Fig. 3). The average particle size increased when longer hydrothermal treatment was applied. The results are summarized in **Table 4**. Comparing these values with the XRD results (**Table 1**), we found that TEM analysis resulted in lower size. The discrepancy is probably due to the fact that TEM gives a number-weighted average of particle size, whereas XRD provides volume-weighted average of crystallite size [34]. The size distribution histograms of PF-TiO<sub>2</sub> NPs (obtained by TEM) in Fig. 3 demonstrate that average values increased while the Gaussian particle size distribution broadened with the increasing treatment time.

### 3.5. EPR investigation of PF-TiO<sub>2</sub> NPs

EPR measurements were performed to detect and identify the reactive oxygen species (ROS) formed by the photoirradiation of the PF-TiO<sub>2</sub> NPs. The reaction of photogenerated short-lived radicals and diamagnetic spin traps leads to the formation of relatively stable paramagnetic radicals, i.e., spin-adducts (Fig. 4).

Hydroxyl radicals (OH·) are regarded as one of the most important reactive species generated upon TiO<sub>2</sub> irradiation in aqueous suspensions and they are frequently detected by EPR method using DMPO as spin trap [21]. This was also the case of our aqueous PF-TiO<sub>2</sub> dispersions: for all PF-TiO<sub>2</sub> samples, characteristic EPR quartet signal (1:2:2:1) of the DMPO-OH adduct was observed. Sample PF-TiO<sub>2</sub>/12 h showed the highest amount OH· radical production, while the partially removing of PF-dopants from the PF-TiO<sub>2</sub> surface upon reaction with NaHCO<sub>3</sub> (see XPS results) led to lower concentration of OH· radicals (Fig. 5a and b). This is in good correlation with our previous assumption that PF-co-doping could effectively enhance the separation of photoinduced charge carriers, therefore increasing their lifetime [25].

DMPO is also commonly used as spin trap to detect superoxide radical anion (O<sub>2</sub>·<sup>−</sup>), nevertheless spin trapping of O<sub>2</sub>·<sup>−</sup> is challenging in aqueous media due to its fast reaction with protons forming H<sub>2</sub>O<sub>2</sub> [35]. Even though in this study the O<sub>2</sub>·<sup>−</sup> formation was not observed in water, its formation can be studied in DMSO which has the ability to stabilize O<sub>2</sub>·<sup>−</sup> [36]. Using the same DMPO and PF-TiO<sub>2</sub> concentration in DMSO, the EPR signal of DMPO-OOH adduct was confirmed (Fig. 6a). While hydrothermal treatment was beneficial to the formation of O<sub>2</sub>·<sup>−</sup>, PF-co-doping seems to hinder the O<sub>2</sub> adsorption on the TiO<sub>2</sub>.

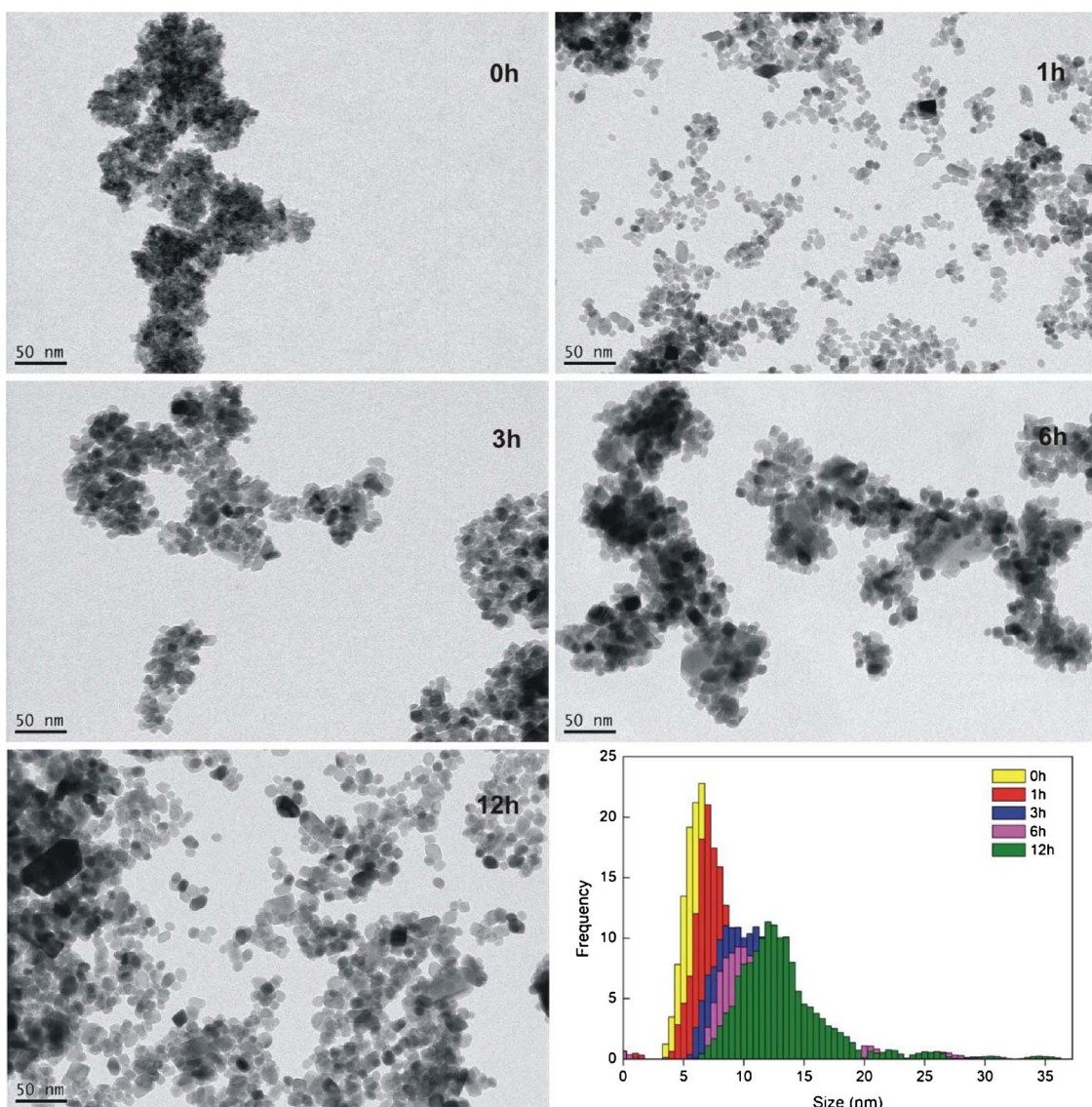


Fig. 3. TEM images and corresponding size distribution histograms of PF-TiO<sub>2</sub> NPs treated hydrothermally at 250 °C for different time periods.

**Table 4**  
The mean diameter  $\pm$  standard deviation values of PF-TiO<sub>2</sub> NPs treated hydrothermally for different time.

Sample ID	Average value (nm)
0 h	6.9 $\pm$ 1.4
1 h	7.6 $\pm$ 2.1
3 h	10.2 $\pm$ 3.2
6 h	12 $\pm$ 4.3
12 h	13.4 $\pm$ 5.8

surface, and hence the O<sub>2</sub><sup>·-</sup> formation. The EPR signal of DMPO-OOH was detectable only after 5–20 min of light irradiation (data not shown) contrary to the reaction rate of hydroxyl radical formation, which was significantly faster. These results are in good agreement with the findings of Lipovsky et al. [35]. Their experiments confirmed that the hydroxyl radicals are principally not derived from O<sub>2</sub><sup>·-</sup> reduction.

The presence of singlet oxygen (<sup>1</sup>O<sub>2</sub>) in the PF-TiO<sub>2</sub> systems was followed by the oxidation of TMPO to 4-oxo-2,2,6,6-tetramethylpiperidine N-oxyl (Tempone). After 20 min of photoirradiation, the EPR triplet of the nitroxide was observable on both sample PF-TiO<sub>2</sub>/12 h and NaHCO<sub>3</sub>-treated PF-TiO<sub>2</sub>/12 h samples but not on PF-TiO<sub>2</sub>/0 h sample (Fig. 6b). From the EPR signal intensity NaHCO<sub>3</sub>-treated PF-

TiO<sub>2</sub>/12 h produced the highest amount of <sup>1</sup>O<sub>2</sub>. Although we cannot exclude the energy transfer mechanism, our data suggest Nosaka's mechanism for the generation of singlet oxygen, when superoxide radical anion is oxidised to it by generated holes at the TiO<sub>2</sub> surface [37].

### 3.6. Photocatalytic activity

The kinetic curves of the photocatalytic degradation of methyl orange (MO) are depicted in Fig. 6c. The lowest reaction rate was observed for the PF-TiO<sub>2</sub>/0 h sample. The rate of photodegradation of MO increased gradually with increasing hydrothermal treatment time. Almost the total decolorization (> 99%) was achieved after 40 min light irradiation by using PF-TiO<sub>2</sub>/12 h sample. At the same time, using PF-TiO<sub>2</sub>/0 h the initial concentration of MO decreased by only 30%. This remarkable difference in their photocatalytic activity shed light on the key role of the crystallinity of the samples which increased with the treatment time as revealed by our XRD measurements. In general, TiO<sub>2</sub> with higher degree of crystallinity, i.e. higher anatase content, contains fewer crystal defects as charge-trapping sites, where the electron-hole recombination can take place [38,39]. Consequently, when the crystallinity is higher the probability of the surface charge-transfer processes can increase. In contrast, amorphous TiO<sub>2</sub> exhibits low

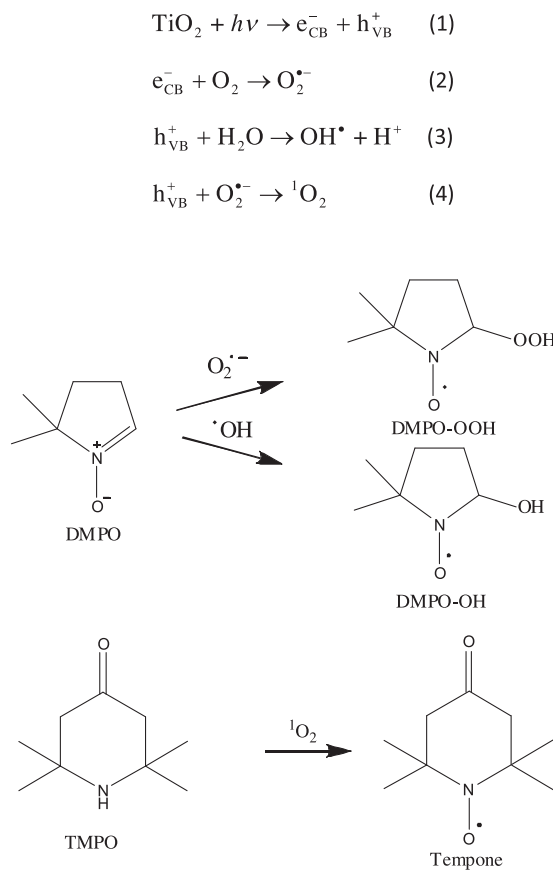


**Fig. 4.** Spin trapping of different ROS formed by the photoinduced reactions on the surface of PF-TiO<sub>2</sub> NPs.

photocatalytic activity even though its specific surface area is very large [40]. As we expected from XRD and TEM results, the specific surface area of our PF-TiO<sub>2</sub> samples decreased from 230 to 93 m<sup>2</sup> g<sup>-1</sup> by the prolonging hydrothermal treatment time from 0 h to 12 h (Table S1). Therefore, PF-TiO<sub>2</sub>/12 h possessed the highest photocatalytic activity with lowest specific surface area. These results confirmed the crucial role of the crystallinity and charge transfer process and also emphasize that large specific surface area is not a sufficient condition for the photocatalytic reactions.

It's interesting to notice that, contrary to what we observed on our anatase PF-TiO<sub>2</sub> NPs, hydrothermal treatment on hierarchically assembled flower-like rutile samples led to lower rate of photodegradation of MO [39]. However, in the presence of H<sub>2</sub>O<sub>2</sub> the highly-crystalline rutile samples showed superior photocatalytic activity. These earlier findings revealed that not only the crystallinity but also the nature of the charge carrier scavengers play crucial role [39]. In this work we have shown that, in the case of anatase PF-TiO<sub>2</sub> NPs dispersions, OH<sup>•</sup> radicals formed by the reaction of photogenerated holes and H<sub>2</sub>O (Eq. (3)) are the major ROS. The capturing of holes by H<sub>2</sub>O on anatase nanoparticles is promoted by both hydrothermal treatment and PF-co-doping. In good agreement with the EPR measurements, the PF-co-doping undoubtedly enhanced OH<sup>•</sup> formation since dopants depletions induced by NaHCO<sub>3</sub> treatment led to lower reaction rate as presented in Fig. 6c. In order to reveal the effects of different dopants, single doped P-TiO<sub>2</sub> and F-TiO<sub>2</sub> NPs were also tested in the degradation of MO. These photocatalysts were synthesized similarly to PF-TiO<sub>2</sub>/12 h, by replacing HPF<sub>6</sub> by H<sub>3</sub>PO<sub>4</sub> or HF and keeping the same P/Ti or F/Ti atomic ratios. Fig. S4 clearly shows the superior photocatalytic activity of PF-TiO<sub>2</sub> relative to F-TiO<sub>2</sub> and P-TiO<sub>2</sub>. This result is indicative for the synergistic effect of P and F co-doping. The reusability tests of PF-TiO<sub>2</sub> photocatalysts were performed in four subsequence

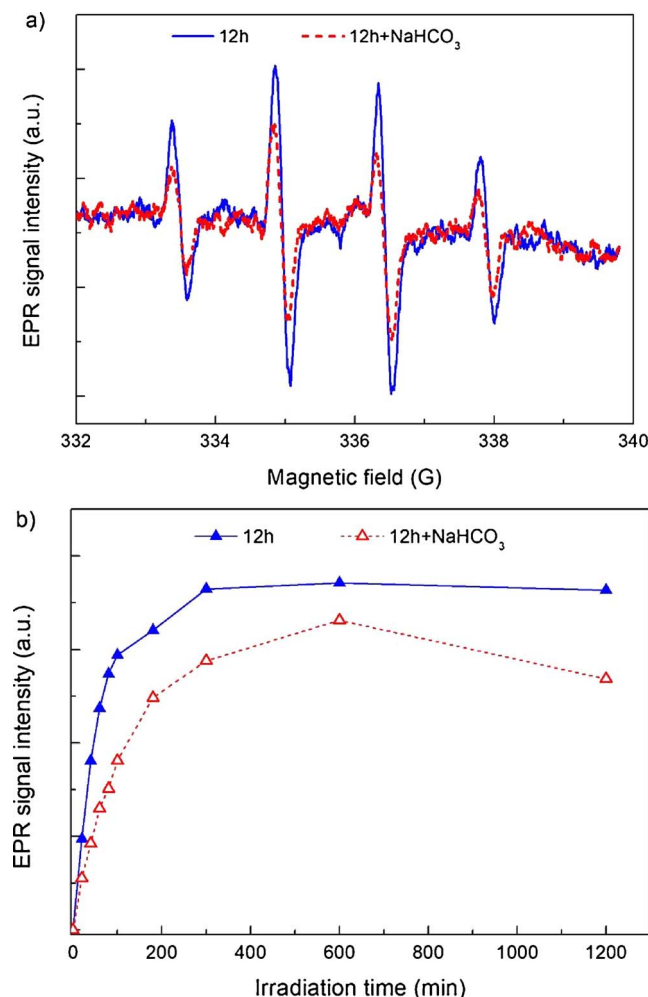


**Fig. 5.** (a) EPR spectra of the DMPO-OH<sup>•</sup> adduct recorded after 100 s light irradiation in aqueous PF-TiO<sub>2</sub>/12 h and NaHCO<sub>3</sub>-treated PF-TiO<sub>2</sub>/12 h NPs dispersions. (b) Formation of the DMPO-OH<sup>•</sup> adduct as a function of irradiation time recorded in aqueous PF-TiO<sub>2</sub>/12 h and NaHCO<sub>3</sub>-treated PF-TiO<sub>2</sub>/12 h NPs dispersions.

cycles. The obtained results showed that the photocatalytic activity did not decrease after reusing the samples (Fig. S5).

### 3.7. Antibacterial activity

We finally tested the antibacterial activity of PF-TiO<sub>2</sub> NPs on CR-Kp 53/3 strain. Our samples did not show antibacterial effects under dark condition, indicating that any possible release of P and/or F dopants do not affect the viability of the bacteria (data not shown). Also, the viable cell number of CR-Kp did not decrease in the absence of photocatalyst even though UV-A irradiation was applied for 60 min. PF-TiO<sub>2</sub>/0 h exhibited the lowest activity under UV-A irradiation, where the living cell number dropped from  $8.1 \times 10^5$  to  $3.4 \times 10^5$  CFU/mL (58% of decrement) in one hour. In the presence of hydrothermally treated PF-TiO<sub>2</sub> NPs, the living cell number of bacteria dropped steeply after 15 min, indicating the high antibacterial activity of these samples (Fig. 6d). The inactivation of bacteria was markedly faster by using PF-TiO<sub>2</sub> than Degussa P25. For PF-TiO<sub>2</sub> NPs, the living cell number dropped from  $\sim 1 \times 10^6$  to  $10^2$  CFU/mL at 30 min. This process led to the elimination of all living bacteria in 45 min. The bactericide effect was very high even though the CR-Kp 53/3 is a capsular type bacteria possessing a characteristic capsule composed of a variable polysaccharide matrix that compass the bacterial cell. This thick and dense layer can protect the bacteria against a broad range of environmental and antimicrobial effects [41].

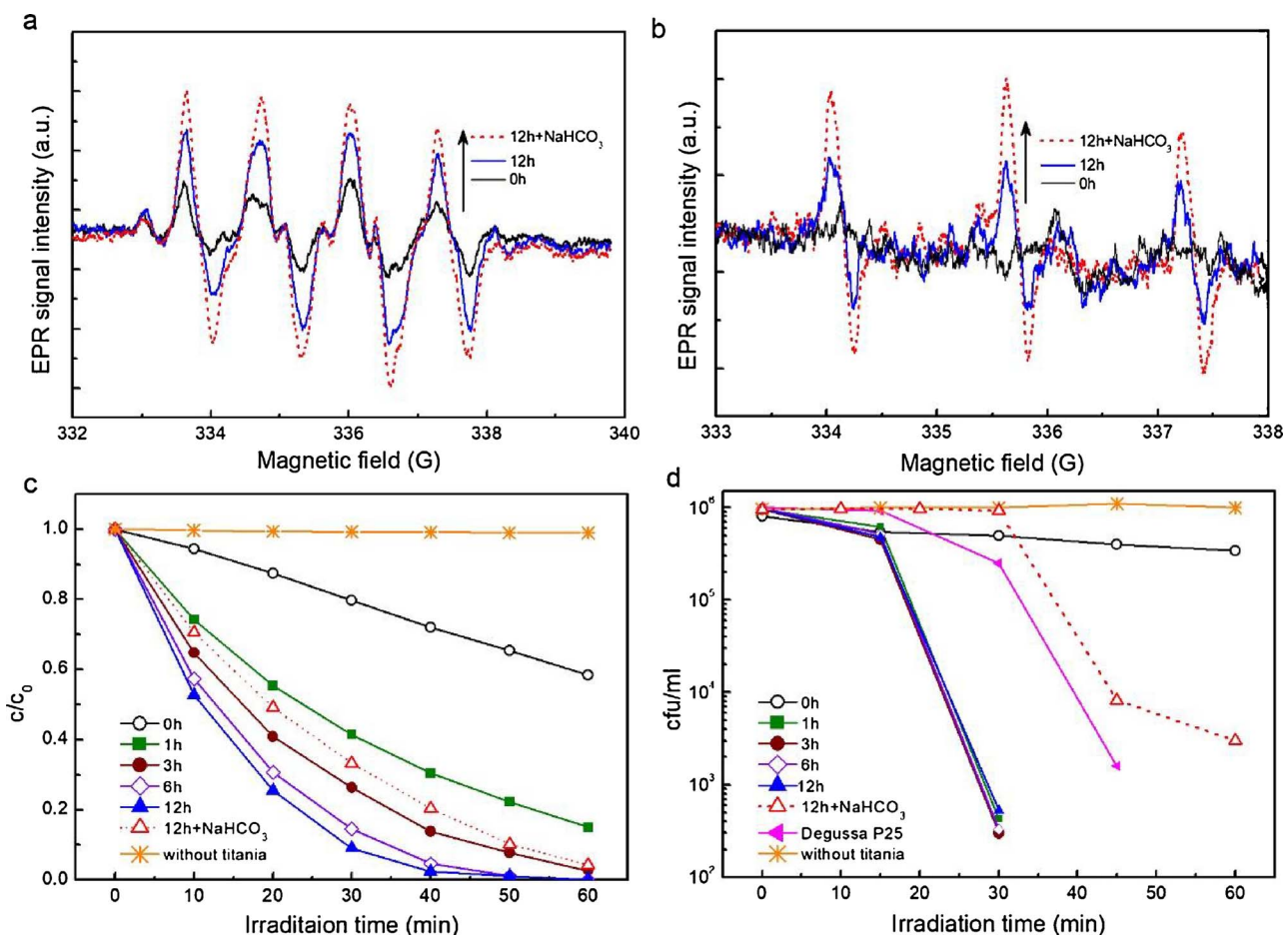


**Fig. 6.** (a) EPR spectra of the DMPO-OOH<sup>\*</sup> adduct recorded after 20 min in DMSO containing different PF-TiO<sub>2</sub> NPs. (b) EPR spectra of Tempone after 45 min light irradiation in different aqueous PF-TiO<sub>2</sub> NPs dispersions. (c) Photocatalytic degradation of methyl orange in aqueous PF-TiO<sub>2</sub> NPs dispersions treated hydrothermally at 250 °C for different time periods. (d) Photocatalytic inactivation of *K. pneumoniae* 53/3 strain in different PF-TiO<sub>2</sub> NPs dispersions.

The observed superior antibacterial activity of PF-TiO<sub>2</sub> NPs probably stems from the enhanced production of OH<sup>·</sup> radicals which is the most reactive ROS. Due to its high reactivity, the proteins, lipids, carbohydrates and DNA can be easily damaged in bacterial cells [42,43]. After partial removing of the dopants from PF-TiO<sub>2</sub>/12 h NPs by using NaHCO<sub>3</sub> treatment, the antibacterial activity significantly decreased as presented in Fig. 6d. This suggests that PF-dopants and thus OH<sup>·</sup> radicals play key role in bactericide effect of PF-TiO<sub>2</sub>. Based on our EPR measurements, NaHCO<sub>3</sub> treatment resulted in lower level of OH<sup>·</sup> which favoured the survival of bacteria, even though the production of O<sub>2</sub><sup>·-</sup> and <sup>1</sup>O<sub>2</sub> was higher at the same time. This finding suggests that antioxidant system of 53/3 strain can defend effectively bacteria against O<sub>2</sub><sup>·-</sup>; and <sup>1</sup>O<sub>2</sub> level is not significant after removing of dopants. It is well known that bacteria can produce superoxide dismutases (SODs) for the elimination of O<sub>2</sub><sup>·-</sup>. Preliminary data (not shown) from the ongoing sequence project of 53/3 has revealed that this strain also contains the three different sod genes such as *sodA* (Mn-type), *sodB* (Fe-type) and *sodC* (Zn-Cu type) with 100% identity to several other *K. pneumoniae* isolates. Role of these genes and their association to the expression of other stress genes will be elucidated in the near future.

The synergistic effect of dopants on the bacteria inactivation was displayed in Fig. S6. Single-doped F-TiO<sub>2</sub> photocatalyst demonstrated much lower antibacterial activity than that of PF-TiO<sub>2</sub>. Even though P-TiO<sub>2</sub> showed photocatalytic activity in the degradation of MO the living cell number did not decrease at all by using this photocatalyst. Interestingly, whereas distinct differences were observed in the photocatalytic activity in degradation of methyl orange, all hydrothermally treated PF-TiO<sub>2</sub> samples (independently on treatment time) exhibited

similarly high killing effects. The difference in the efficacy between the dye degradation and bacterial inactivation has not been clarified yet. Complex cells, such as bacteria, can limit the killing effect of TiO<sub>2</sub> NPs in a number of ways. Further studies are necessary to clarify the background of antibacterial effects of PF-TiO<sub>2</sub>.

#### 4. Conclusions

In this paper, we demonstrated that multidrug resistant CR-Kp can be effectively inactivated by using hydrothermally treated PF-co-doped anatase TiO<sub>2</sub> NPs.

We carefully evaluated the influence of the hydrothermal treatment on the evolution of structure, morphology and elemental composition of our PF-TiO<sub>2</sub> NPs over periods up to 12 h. We found that hydrothermal treatment increased the particle size and the crystallinity of PF-TiO<sub>2</sub> NPs meanwhile the morphology did not change significantly. Based on our detailed XPS study, we observed a gradual decrease of F<sup>-</sup> content as a function of treatment duration, while P<sup>5+</sup> ions concentration remained almost constant, suggesting that whereas F adsorbed on the surface of TiO<sub>2</sub>, P can enter into the lattice. Hydrothermal treatment on PF-TiO<sub>2</sub> NPs increased both their photocatalytic and antibacterial activities by promoting the formation of ROS. Removing of PF-dopants led to decreasing photocatalytic and antibacterial activity even though the level of O<sub>2</sub><sup>·-</sup> radicals and <sup>1</sup>O<sub>2</sub> increased at the same time. Consequently, we attributed the superior photocatalytic activity of our PF-TiO<sub>2</sub> NPs to the increased OH<sup>·</sup> radicals generation leading to the rapid inactivation of capsular type carbapenem-resistant *K. pneumoniae*. Our kinetic investigation on the hydrothermal treatment

revealed that PF-TiO<sub>2</sub> NPs with high antibacterial activity can be prepared at relatively low temperature and with short synthesis time. PF-co-doping of TiO<sub>2</sub> is an effective tool to manipulate the ROS formation and synthesize highly efficient photocatalysts. PF-co-doping can be a part of multi-elements doping to produce visible-light active TiO<sub>2</sub> with high oxidation ability.

## Acknowledgments

This paper was supported by the János Bolyai Research Scholarship of the Hungarian Academy of Sciences. Support from National Research, Development and Innovation Office (OTKA FK 124331) are also gratefully acknowledged.

## Appendix A. Supplementary data

Supplementary material related to this article can be found, in the online version, at doi:<https://doi.org/10.1016/j.apcatb.2018.03.012>.

## References

- [1] E.B. Hirsch, V.H. Tam, Detection and treatment options for Klebsiella pneumoniae carbapenemases (KPCs): an emerging cause of multidrug-resistant infection, *J. Antimicrob. Chemother.* 65 (2010) 1119–1125.
- [2] R.P. Gaynes, D.H. Culver, Resistance to imipenem among selected gram-negative bacilli in the united states, *Infect. Control Hosp. Epidemiol.* 13 (1992) 10–14.
- [3] M.A. Schembri, J. Blom, K.A. Kroghfelt, P. Klemm, Capsule and fimbria interaction in Klebsiella pneumoniae, *Infect. Immun.* 73 (2005) 4626–4633.
- [4] O. Carp, C.L. Huisman, A. Reller, Photoinduced reactivity of titanium dioxide, *Prog. Solid State Chem.* 32 (2004) 33–177.
- [5] K. Nakata, A. Fujishima, TiO<sub>2</sub> photocatalysis: design and applications, *J. Photochem. Photobiol. C: Photochem. Rev.* 13 (2012) 169–189.
- [6] P.C. Maness, S. Smolinski, D.M. Blake, Z. Huang, E.J. Wolfrum, W.A. Jacoby, Bactericidal activity of photocatalytic TiO<sub>2</sub> reaction: toward an understanding of its killing mechanism, *Appl. Environ. Microbiol.* 65 (1999) 4094–4098.
- [7] C.D. Valentini, G. Pacchioni, Trends in non-metal doping of anatase TiO<sub>2</sub>: B, C, N and F, *Catal. Today* 206 (2013) 12–18.
- [8] Z. Hu, Z. Shen, J.C. Yu, Phosphorus containing materials for photocatalytic hydrogen evolution, *Green Chem.* 19 (2017) 588–613.
- [9] Y. Lv, L. Yu, H. Huang, H. Liu, Y. Feng, Preparation, characterization of P-doped TiO<sub>2</sub> nanoparticles and their excellent photocatalytic properties under the solar light irradiation, *J. Alloys Compd.* 488 (2009) 314–319.
- [10] L. Körösi, A. Oszkó, G. Galbács, A. Richardt, V. Zöllmer, I. Dékány, Structural properties and photocatalytic behaviour of phosphate-modified nanocrystalline titania films, *Appl. Catal. B* 77 (2007) 175.
- [11] L. Körösi, S. Papp, I. Bertóti, I. Dékány, Surface and bulk composition, structure, and photocatalytic activity of phosphate-modified TiO<sub>2</sub>, *Chem. Mater.* 19 (2007) 4811–4819.
- [12] M. Pelaez, N.T. Nolan, S.C. Pillai, M.K. Seery, P. Falaras, A.G. Kontos, P.S.M. Dunlop, J.W.J. Hamilton, J.A. Byrne, K. O'Shea, M.H. Entezari, D.D. Dionysiou, A review on the visible light active titanium dioxide photocatalysts for environmental applications, *Appl. Catal. B* 125 (2012) 331–349.
- [13] Y. Li, W. Wang, X. Qiu, L. Song, H.M. Meyer III, M.P. Paranthaman, G. Eres, Z. Zhang, B. Gu, Comparing Cr, and N only doping with (Cr, N)-codoping for enhancing visible light reactivity of TiO<sub>2</sub>, *Appl. Catal. B* 110 (2011) 148–153.
- [14] M.V. Dozzi, E. Sellia, Doping TiO<sub>2</sub> with p-block elements: effects on photocatalytic activity, *J. Photochem. Photobiol. C: Photochem. Rev.* 14 (2013) 13–28.
- [15] X. Li, J. Shi, H. Chen, R. Wan, C. Leng, S. Chen, Y. Lei, A DFT study on the modification mechanism of (Cr, C) co-doping for the electronic and optical properties of anatase TiO<sub>2</sub>, *Comput. Mater. Sci.* 129 (2017) 295–303.
- [16] J. Zhang, K. Tse, M. Wong, Y. Zhang, J. Zhu, A brief review of co-doping, *Front. Phys.* 11 (2016) 117405.
- [17] Q.L. Liu, Z.Y. Zhao, Q.J. Liu, Synergistic effects of nonmetal co-doping with sulfur in anatase TiO<sub>2</sub>: a DFT + U study, *Phys. Chem. Chem. Phys.* 17 (2015) 3426–3434.
- [18] A. Chatzitakis, M. Grandcolas, K. Xu, S. Mei, J. Yang, I.J.T. Jensen, C. Simon, T. Norby, Assessing the photoelectrochemical properties of C, N, F codoped TiO<sub>2</sub> nanotubes of different lengths, *Catal. Today* 287 (2017) 161–168.
- [19] A. Samokhvalov, Hydrogen by photocatalysis with nitrogen codoped titanium dioxide, *Renew. Sustain. Energy Rev.* 72 (2017) 981–1000.
- [20] L. Lin, R.Y. Zheng, J.L. Xie, Y.X. Zhu, Y.C. Xie, Synthesis and characterization of phosphor and nitrogen co-doped titania, *Appl. Catal. B: Environ.* 76 (2007) 196–202.
- [21] Z. Wang, W. Ma, C. Chen, H. Ji, J. Zhao, Probing paramagnetic species in titanate-based heterogeneous photocatalysis by electron spin resonance (ESR) spectroscopy—a mini review, *Chem. Eng. J.* 170 (2011) 353–362.
- [22] O. Elbanna, P. Zhang, M. Fujitsuka, T. Majima, Facile preparation of nitrogen and fluorine codoped TiO<sub>2</sub> mesocrystal with visible light photocatalytic activity, *Appl. Catal. B: Environ.* 192 (2016) 80–87.
- [23] P. Zheng, H. Wu, J. Guo, J. Dong, S. Jia, Z. Zhu, P-N co-doping induced structural recovery of TiO<sub>2</sub> for overall water splitting under visible light irradiation, *J. Alloys Compd.* 615 (2014) 79–83.
- [24] G. Yang, T. Wang, B. Yang, Z. Yan, S. Ding, T. Xiao, Enhanced visible-light activity of P-N co-doped TiO<sub>2</sub> nanocrystals via nonmetal impurity, Ti<sup>3+</sup> ions and oxygen vacancies, *Appl. Surf. Sci.* 287 (2013) 135–142.
- [25] L. Körösi, M. Prato, A. Scarpellini, A. Riedinger, J. Kovács, M. Kus, V. Meynen, S. Papp, Hydrothermal synthesis, structure and photocatalytic activity of PF-codoped TiO<sub>2</sub>, *Mater. Sci. Semicond. Process* 30 (2015) 442–450.
- [26] R. Bonnett, R.F.C. Brown, V.M. Clark, I.O. Sutherland, A. Todd, Experiments towards the synthesis of corrins. Part II. The preparation and reactions of  $\Delta^1$ -pyrroline 1-oxides, *J. Chem. Soc.* (1959) 2094–2102.
- [27] L. Körösi, D. Dömötör, S. Beke, M. Prato, A. Scarpellini, K. Meczker, G. Schneider, T. Kovács, Á. Kovács, S. Papp, Antibacterial activity of nanocrystalline TiO<sub>2</sub>(B) on multiresistant Klebsiella pneumoniae strains, *Sci. Adv. Mater.* 5 (2013) 1184–1192.
- [28] N. Gleason, J. Guevremont, F. Zaera, Thermal chemistry of 2-propanol and 2-propyl iodide on clean and oxygen-pre-treated Ni(100) single-crystal surfaces, *J. Phys. Chem. B* 107 (2003) 11133–11141.
- [29] J. Matharu, G. Cabailh, G. Thornton, Synthesis of TiO<sub>2</sub>(110) ultra-thin films on W(100) and their reactions with H<sub>2</sub>O, *Surf. Sci.* 616 (2013) 198–205.
- [30] L. Junqi, W. Defang, L. Hui, H. Zuoli, Z. Zhenfeng, Synthesis of fluorinated TiO<sub>2</sub> hollow microspheres and their photocatalytic activity under visible light, *Appl. Surf. Sci.* 257 (2011) 5879–5884.
- [31] Q. Shi, D. Yang, Z. Jiang, J. Li, Visible-light photocatalytic regeneration of NADH using P-doped TiO<sub>2</sub> nanoparticles, *J. Mol. Catal. B: Enzym.* 43 (2006) 44–48.
- [32] Q. Zhu, Y. Peng, L. Lin, C.-M. Fan, G.-Q. Gao, R.-X. Wang, A.-W. Xu, Stable blue TiO<sub>2-x</sub> nanoparticles for efficient visible light photocatalysts, *J. Mater. Chem. A* 2 (2014) 4429–4437.
- [33] T.R. Gordon, M. Cargnello, T. Paik, F. Mangolini, R.T. Weber, P. Fornasiero, C.B. Murray, Nonaqueous synthesis of TiO<sub>2</sub> nanocrystals using TiF<sub>4</sub> to engineer morphology, oxygen vacancy concentration, and photocatalytic activity, *J. Am. Chem. Soc.* 134 (2012) 6751–6761.
- [34] T. Hyde, Crystallite size analysis of supported platinum catalysts by XRD, *Platinum Met. Rev.* 52 (2008) 129–130.
- [35] D. Dvoranová, Z. Barbierková, V. Brezová, Radical intermediates in photoinduced reactions on TiO<sub>2</sub> (an EPR spin trapping study), *Molecules* 19 (2014) 17279–17304.
- [36] A. Lipovsky, L. Levitski, Z. Tzitrinovich, A. Gedanken, R. Lubart, The different behavior of rutile and anatase nanoparticles in forming oxy radicals upon illumination with visible light: an EPR study, *Photochem. Photobiol.* 88 (2012) 14–20.
- [37] T. Daimon, Y. Nosaka, Formation and behavior of singlet molecular oxygen in TiO<sub>2</sub> photocatalysis studied by detection of near-infrared phosphorescence, *J. Phys. Chem. C* 111 (2007) 4420–4424.
- [38] A. Kudo, Y. Misaki, Heterogeneous photocatalyst materials for water splitting, *Chem. Soc. Rev.* 38 (2009) 253–278.
- [39] L. Körösi, M. Prato, A. Scarpellini, J. Kovács, D. Dömötör, T. Kovács, S. Papp, H<sub>2</sub>O<sub>2</sub>-assisted photocatalysis on flower-like rutile TiO<sub>2</sub> nanostructures: rapid dye degradation and inactivation of bacteria, *Appl. Surf. Sci.* 365 (2016) 171–179.
- [40] J. Yu, Y. Su, B. Cheng, Template-free fabrication and enhanced photocatalytic activity of hierarchical macro-/mesoporous titania, *Adv. Funct. Mater.* 17 (2007) 1984–1990.
- [41] C. March, V. Cano, D. Moranta, E. Llobet, C. Pérez-Gutiérrez, J.M. Tomás, T. Suárez, J. Garmendia, J.A. Bengoechea, Role of bacterial surface structures on the interaction of Klebsiella pneumoniae with phagocytes, *PLoS One* 8 (2013) e56847.
- [42] E. Cabiscol, J. Tamarit, J. Ros, Oxidative stress in bacteria and protein damage by reactive oxygen species, *Int. Microbiol.* 3 (2000) 3–8.
- [43] B. Ezraty, A. Gennaris, F. Barras, J.F. Collet, Oxidative stress, protein damage and repair in bacteria, *Nat. Rev. Microbiol.* 15 (2017) 385–396.